Computers and Concrete, *Vol. 16, No. 1 (2015) 17-35*
DOI: http://dx.doi.org/10.12989/cac.2015.16.1.017

Comparison of linear and non-linear earthquake response of masonry walls

Erkut Sayın* and Yusuf Calayır

Department of Civil Engineering, Fırat University, Elazığ, Turkey

(Received January 22, 2015, Revised June 18, 2015, Accepted June 22, 2015)

Abstract. In this study, linear and non-linear response of a masonry wall that includes an opening was presented. The masonry wall was modeled with two-dimensional finite elements. Smeared crack model that includes the strain softening behavior was selected to the masonry wall material. For the numerical application, linear and non-linear analyses of the masonry wall were carried out using east-west and vertical components of the 1992 Erzincan and 2003 Bingöl earthquake acceleration records. Linear and non-linear solutions were compared each other. The displacement and stress results at the selected points of the masonry wall and crack propagation in the masonry wall were presented for both earthquake acceleration records.

Keywords: masonry wall; non-linear analysis; smeared crack model

1. Introduction

A substantial percentage of Turkey's surface area is located on a seismic belt; therefore the majority of Turkey's population lives in structures that are located in first- and second- degree seismic zones. According to the building census performed by the State Institute of Statistics in the year 2000, masonry structures constitute 51% of the buildings in Turkey (Building Census 2000). Substantial number of these structures is in rural regions and the outskirts of cities. Masonry structures are more economical and preferred over other structure systems because the relevant materials can be easily obtained and their construction and workmanship are easier. For this reason, the ratio of masonry structures increase to 82% in rural regions (Erdik and Aydınoğlu 2003). Masonry structures are construction systems where walls, comprised of mortar and masonry units such as briquette, brick, stone and adobe, are used as the load-bearing system. Most of these buildings were constructed without receiving any engineering services and were severely damaged during earthquakes. Many studies concerning the about failure of masonry buildings have been conducted by many researchers, such as Klingner (2006), Bayraktar *et al.* (2007), Naseer *et al.* (2010), Ingham and Griffith (2011), Calayır *et al.* (2012), Sayın *et al.* (2013) and Sayın *et al.* (2014). Fig. 1 presents the failure mode of masonry walls with an opening.

The most important structural elements for masonry structures are the load-bearing walls. Three

* Corresponding author, Assistant professor, E-mail: erkutsayin@gmail.com

http://www.techno-press.org/?journal=cac&subpage=8 ISSN: 1598-8198 (Print), 1598-818X (Online)

modeling techniques, detailed micro modeling, simplified micro modeling and macro modeling (see Fig. 2), are used depending on the sensitivity level and requested simplicity in the modeling of masonry (Lourenço 1996).

Material specifications of masonry units and mortar, namely, the modulus of elasticity and Poisson's ratio, are evaluated separately in the detailed micro modeling technique. This modeling technique is one of the best modeling techniques for modeling the behaviors of masonry walls. However, it needs greater computational effort. This modeling technique is particularly suitable for small structures or for the solution of a part of the structure. The dimensions of masonry units expand by as much as half of the thickness of the mortar layer, and the mortar layer is ignored in simplified micro modeling. The masonry units are separated from one another through the interfacial lines. The cracks that occur in the system are expected to occur in these interfacial lines. Macro modeling is an equivalent material model that accepts the masonry as a composite without making a distinction between stone, brick and mortar. This technique is preferable because it significantly decreases the computer solution time. This modeling technique is the most common technique for analysis of full-scale masonry models. Because of its low computational effort, this technique is used in the literature (Modena *et al.* 2002, Carpinteri *et al.* 2005, Bernardeschi *et al.* 2004, Bayraktar *et al.* 2010, Ivorra *et al.* 2010 and Unnikrishnan *et al.* 2013). One modelling strategy cannot be preferred over the other because different application fields exist for micro and macro models.

Fig. 1 Failure modes of masonry walls with an opening

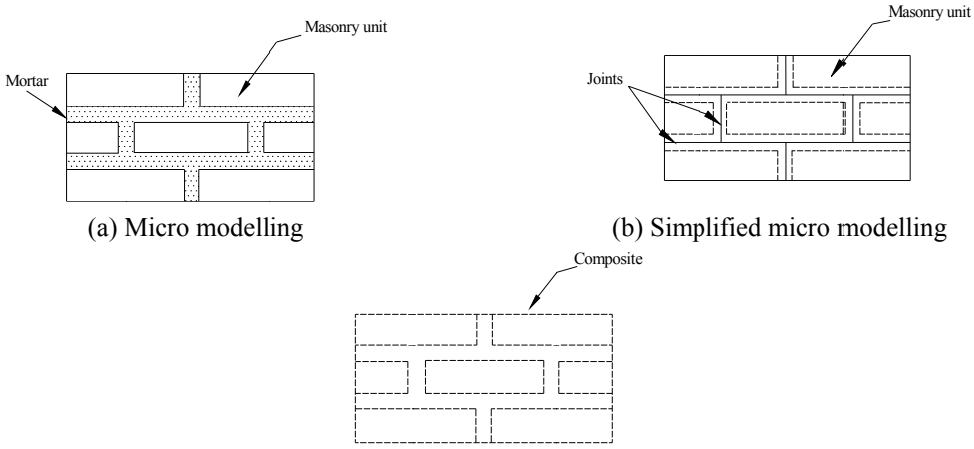

(a) Micro modelling

(b) Simplified micro modelling

(c) Macro modeling

Fig. 2 Masonry wall modelling techniques

2. Smeared crack approach

In fracture mechanics, cracks are investigated using two different approaches: discrete and smeared. In the discrete crack approach, a crack occurs when the calculated tensile stresses exceed the material tensile strengths, and in the finite element system, the calculation is continued by taking two nodal points instead of one by opening the gap between two elements where the crack has occurred. New node points to be added in the finite element system with the crack formation, increasing number of freedom degree in the system and extension of the band width are the disadvantages of the method (Skrikerud and Bachmann 1986). In the smeared crack model, cracks occur normal to principal tensile stress, if the maximum principal tensile stress of an element, calculated in Gauss integration point, exceeds its tensile strength. It is assumed that tensile strengths perpendicular to crack cannot be compensated after crack formation at the integration point; the matrix between stress and strain at that point has been modified. This matrix is expressed according to local axes set defined on the crack plane. The dimension of the stiffness matrix remains constant because no new nodes are defined in the system. This is an advantage of the smeared crack model. The disadvantage of this model is that detailed information about the geometry of the cracks cannot be obtained. Nonlinear properties, such as shear and cracking of an element, can be considered in this approach. The smeared crack model separates into two models: fixed and rotating smeared crack models (Rots 1988). Because the crack direction remains stable at the integration point during the analysis in the fixed model, the crack direction exhibits a constant change at the relevant integration point in the rotating model. Although the smeared crack model was first developed for the numerical modeling of concrete structures, it can also be used in the analysis of masonry structures (Rots 1991, Lofti and Shing 1991, Shing and Cao 1997). In this study, the smeared crack model that considers strain softening for material behavior has been used. It is possible to determine the material behavior in this model as that before the strain softening, during the strain softening and after the strain softening.

2.1 Behavior before strain softening

The following relation holds between the plane stress and strain anywhere in the material in the finite element analysis (Eq. (1))

$$\{\sigma\}=[D]\{\varepsilon\} \tag{1}$$

Here, $\{\sigma\}$ and $\{\varepsilon\}$ are the vectors of stress and strain, respectively. $[D]$ represents the constitutive matrix. For a plane stress, $[D]$ matrix for a plane stress can be expressed in the following form for a linear elastic and isotropic material (Eq. (2)).

$$[D] = \frac{E}{1-\nu^2}\begin{bmatrix} 1 & \nu & 0 \\ \nu & 1 & 0 \\ 0 & 0 & \dfrac{(1-\nu)}{2} \end{bmatrix} \tag{2}$$

In this form, E is the modulus of elasticity, and ν is Poisson's ratio.

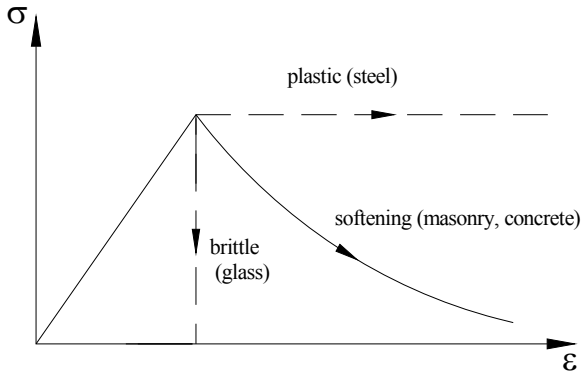

Fig. 3 Stress-deformation behavior of various materials (Rots 1997)

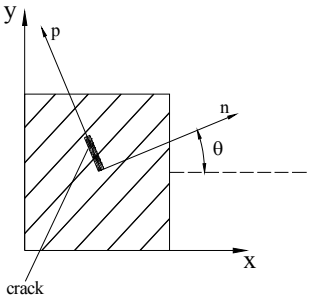

Fig. 4 Local axes

2.2 Behavior during strain softening

When the tensile stresses approach to maximum strength, micro cracking is initiated in the material. After the maximum strength limit is exceeded, a gradual decrease in the stress occurs with the extension and conjunction of the current cracks. This behavior of the material is called as strain softening. The stress-deformation behavior of various materials is given in Fig. 3.

The smeared micro crack band occurs perpendicularly to principal tensile strain direction (Fig. 4). The material reference axes, which are called the local axes, are chosen in the same direction as the principal strain.

The stress-strain matrix in the local axes is defined as Eq. (3) (Lubliner *et al.* 1989)

$$[D]_{ns} = \begin{bmatrix} \frac{E\eta}{1-\eta\nu^2} & \frac{E\eta\nu}{1-\eta\nu^2} & 0 \\ \frac{E\eta\nu}{1-\eta\nu^2} & \frac{E}{1-\eta\nu^2} & 0 \\ 0 & 0 & \mu\frac{E}{2(1+\nu)} \end{bmatrix} \qquad \eta = \frac{E_n}{E} \tag{3}$$

In this equation, η ($0 \leq \eta \leq 1$) parameter represents the ratio of the softened modulus of elasticity (E_n) perpendicular to the crack plane to the initial elastic modulus of elasticity (E). In

addition, μ is the shear resistance factor and can be defined as in Eq. 4 in the rotating crack model.

$$\mu = \frac{1+\nu}{1-\eta\nu^2}\left(\frac{\eta\varepsilon_n - \varepsilon_p}{\varepsilon_n - \varepsilon_p} - \eta\nu\right) \tag{4}$$

Here ε_n and ε_p represent normal strains perpendicular and parallel to the fracture plane, respectively. [D_{np}] matrix, obtained using the local axes, is converted into a matrix [D_{xy}] (Eq. (5)) in the global axes via a transformation matrix.

$$[D_{xy}] = [T]^T [D_{np}][T] \tag{5}$$

In Eq. (5), [T] is the transformation matrix, and this matrix is given by Eq. (6). In this equation, θ represents maximum principal strain direction.

$$T = \begin{bmatrix} \cos^2\theta & \sin^2\theta & \sin\theta\cos\theta \\ \sin^2\theta & \cos^2\theta & -\sin\theta\cos\theta \\ -2\sin\theta\cos\theta & 2\sin\theta\cos\theta & \cos^2\theta - \sin^2\theta \end{bmatrix} \tag{6}$$

2.3 Behavior after strain softening (closing and reopening of cracks)

Softening behavior is a typical characteristic for semi-brittle materials, such as brick, mortar, ceramic and concrete. With the increase of strain in the softening zone, the softened modulus of elasticity (E_n) as well as η and μ gradually decrease and may become zero after complete fracturing ($\varepsilon_n > \varepsilon_{cr}$). At this stage, Eq. (3), which defines the stress-strain matrix in the local axes, is updated using the new values of the above parameters. The closing and reopening of cracks are shown in Fig. 5.

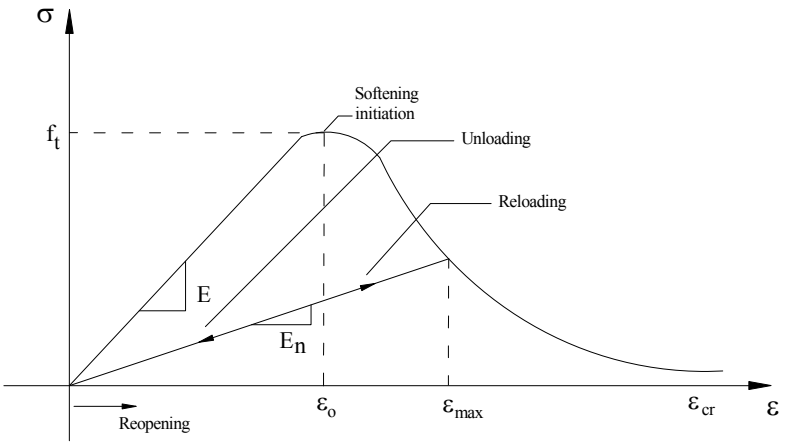

Fig. 5 Closing and reopening of cracks

The following equations (Eqs. (7a) and (7b)) are used in the stress-strain curve given in Fig. 5

$$\sigma(\varepsilon)=E\,\varepsilon, \qquad \varepsilon \le \varepsilon_o \tag{7a}$$

$$\sigma(\varepsilon)= f_t\left[2e^{-a(\varepsilon-\varepsilon_o)}-e^{-2a(\varepsilon-\varepsilon_o)}\right], \qquad \varepsilon_o \le \varepsilon \le \varepsilon_{cr} \tag{7b}$$

The value of ε_n, the normal strain value, may either increase or decrease under seismic loading calculated at the relevant integration point. Therefore, opening or closing may occur at the crack. The state of being open or closed of crack is determined based on the calculated value of ε_n perpendicular to the crack plane at the relevant integration point of an element that was also previously cracked. Accordingly, when the calculated normal strain value is greater than zero, it is accepted that the crack is open. If the calculated normal strain value is less than or equal to zero, then it is accepted that the crack is closed, and the softened modulus of elasticity varies with the initial modulus of elasticity E. During unloading/reloading, if ε_n strain value perpendicular to the crack plane at the relevant integration point of an element, which was previously cracked, does not exceed $\varepsilon_{\max}$ value, which is indicated in Fig. 5, then a new secant modulus value E_n is not recalculated, and the previous value is considered. However, if this value exceeds $\varepsilon_{\max}$ value, a new E_n value is calculated, and the procedure continues in this manner. For all of the situations mentioned above, [D_{np}] constitutive matrix is updated. In Fig. 5, ε_{cr} indicates completely fractured strain. ε_{cr} is defined as in Eq. (8) in finite element calculations.

$$\varepsilon_{cr} = \varepsilon_o + \frac{\ln\left(\dfrac{1+\sqrt{1-\delta}}{\delta}\right)}{a} \tag{8}$$

In this equation, δ is taken to be equal to $0.02\,f_t$. Therefore, Eq. (8) transforms into the following (Eq. (9)).

$$\varepsilon_{cr} = \varepsilon_o + \frac{4.6}{a} \tag{9}$$

Here, a value is a non-dimensional constant and can be defined with the equation below (Lubliner *et al.* 1989).

$$a = \frac{3}{\varepsilon_o\left[\dfrac{2EG_f}{l_{ch}f_t^{\,2}}-1\right]} \tag{10}$$

In Eq. (10), l_{ch} represents the characteristic element dimension, G_f represents fracture energy, and f_t represents the tensile strength of the materials. The uniaxial stress–strain is shown in Fig. 6.

The characteristic element dimension is the ratio of the fracture energy (G_f) to the energy per unit volume (g_f) (Bazant and Cabot 1989). Here, g_f defines the total area that remains under

stress–strain curve (Eq. (11)).

$$g_f = \frac{G_f}{l_{ch}} \tag{11}$$

3. Numerical solution of the equation of motion

The non-linear equation of motion for damped structural systems can be written as follows (Eq. (12))

$$[M]\{a\}+[C]\{v\}+\{F^i\}=\{F\} \tag{12}$$

Here, $[M]$ and $[C]$ represent the mass and damping matrixes, respectively. In addition, $\{F^i\}$ and $\{F\}$ represent the resisting and external force vectors, respectively. In case of earthquake ground motion, the external force vector is expressed as below (Eq. (13)).

$$\{F\}=\{F^{sta}\}-[M]\{a_g\} \tag{13}$$

In this equation, $\{F^{sta}\}$ represents the static load vector of the system, and $\{a_g\}$ represents the ground motion acceleration vector. Stiffness proportional damping is considered in the structural system. In this case, the damping matrix is written as (Eq. (14)),

$$[C]=b[K] \tag{14}$$

Here $[K]$ is the stiffness matrix, and b is the proportion factor that is based on the damping ratio used in the fundamental mode of the structure. The HHT-α algorithm, suggested by Miranda *et al.* (1989), was used to numerically solve the equation of motion. This algorithm is based on Newmark's average acceleration method. With i the time step in Newmark's method, Eqs. (15) and (16) are used for the displacement and velocity at the (i+1) th time step, respectively.

$$u_{i+1} = u_i + \Delta t\, v_i + \frac{1}{2}\Delta t^2 [(1-2\beta)a_i + 2\beta\, a_{i+1}] \tag{15}$$

$$v_{i+1} = v_i + \Delta t\, [(1-\gamma)a_i + \gamma\, a_{i+1}] \tag{16}$$

In these equations, u, v and a are the displacement, velocity and acceleration, respectively; β and γ are Newmark's coefficients; and Δt is the integration time step. Using the integration algorithm, the equation of motion of the system given by Eq. (12) can be rewritten as follows Eq. (17) (Rots 1997).

$$[M]\{a\}_{i+1} + (1+\alpha)[C]\{v\}_{i+1} - \alpha[C]\{v\}_i + (1+\alpha)\{F^i\}_{i+1} - \alpha\{F^i\}_i = (1+\alpha)\{F\}_{i+1} - \alpha\{F\}_i \tag{17}$$

Here, α is a parameter that controls the numerical damping. The coefficients should be chosen as below, thereby controlling the unconditional stability and second order accuracy (Eq. (18)).

$$\alpha \in [\frac{-1}{3}, 0] \qquad \beta = \frac{1}{4}(1-\alpha^2) \qquad \gamma = \frac{1}{2} - \alpha \tag{18}$$

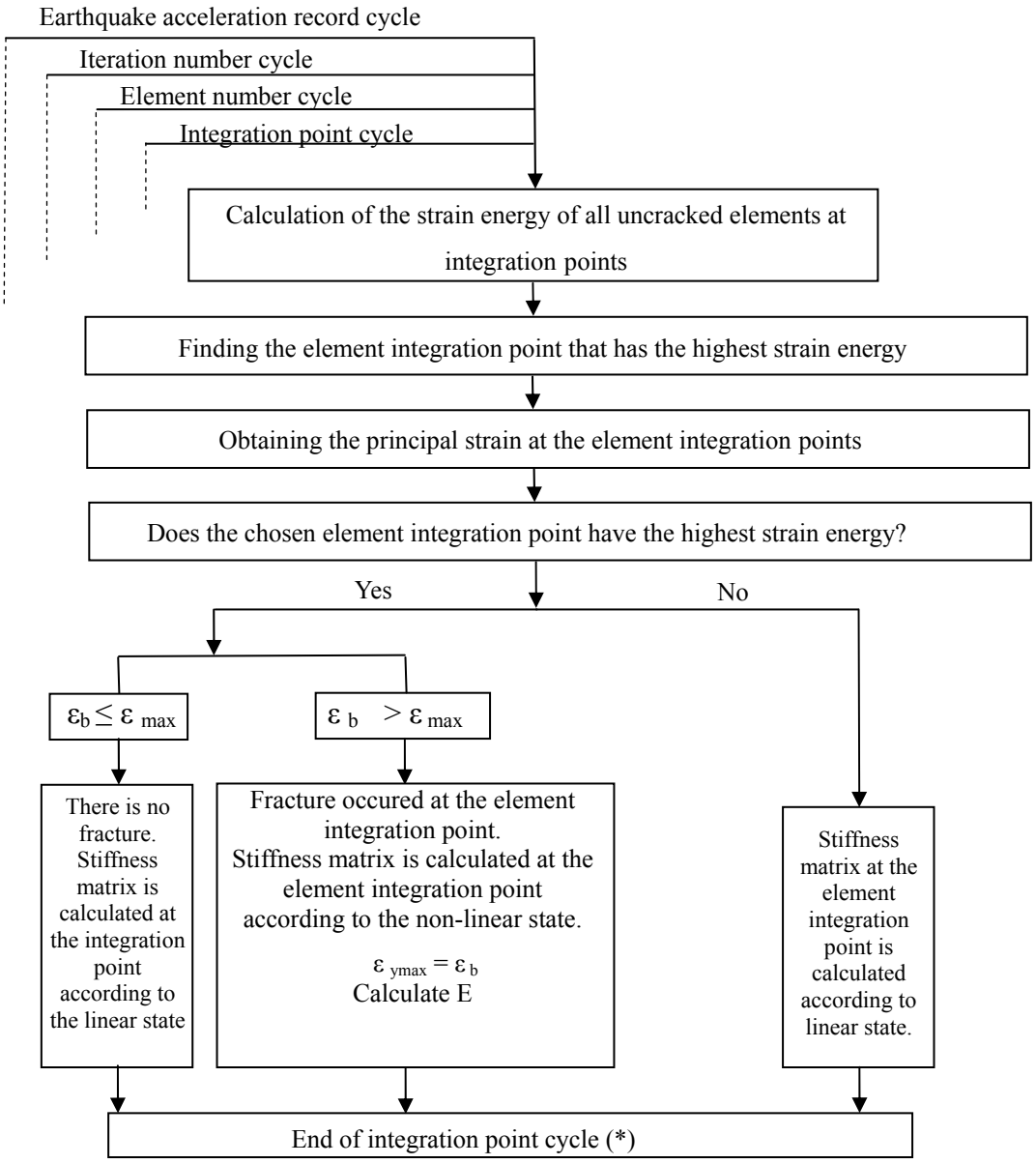

Fig. 7 Dynamic analysis flow diagram

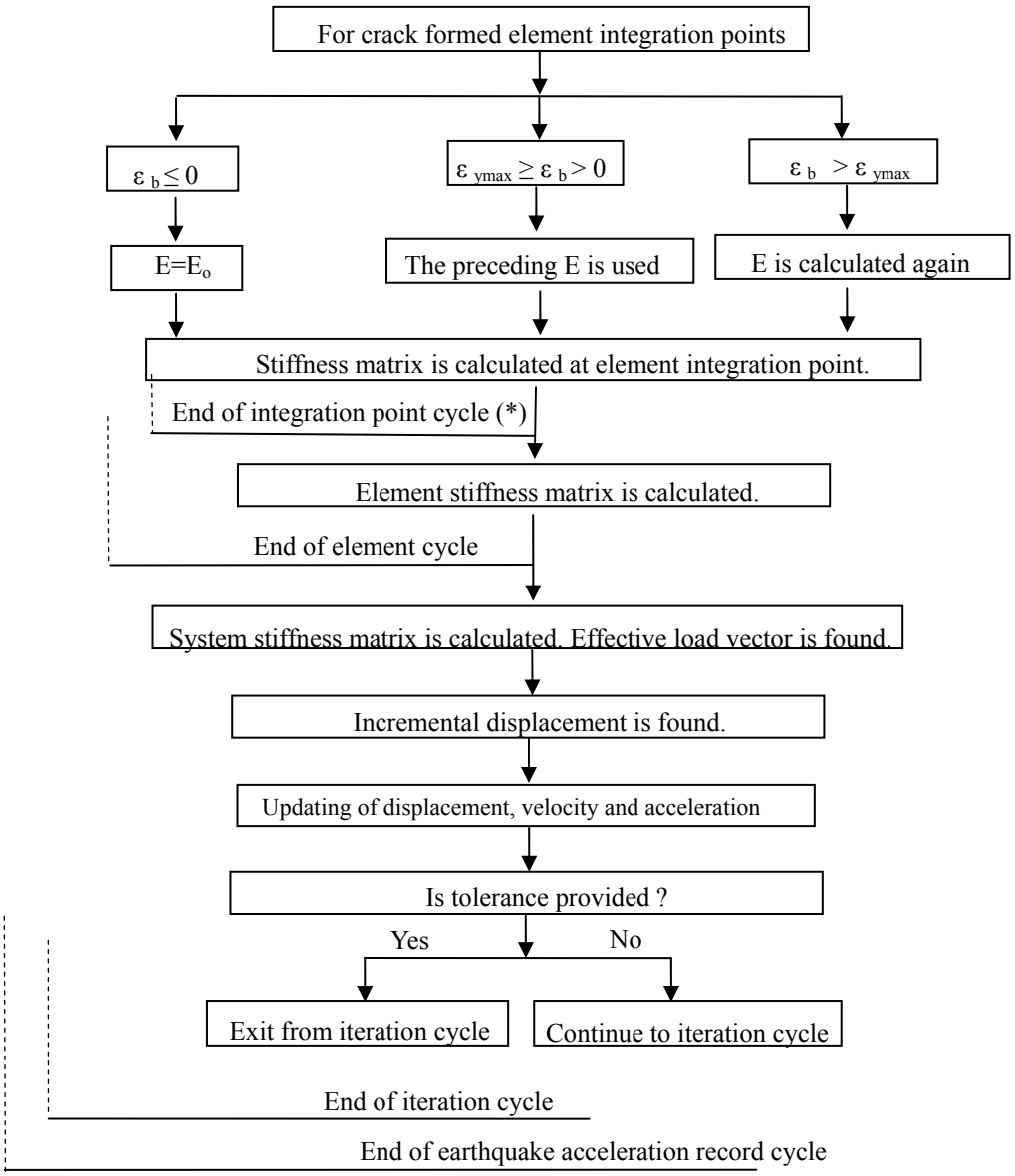

Fig. 8 Dynamic analysis flow diagram (cont.)

To solve the non-linear equations of motion, predictor corrector method is used together with the Newton-Raphson method. If the solutions at time step i are known, the estimated displacement and velocity vectors for time step i+1 are calculated as follows: (Eqs. (19) and (20))

$$\{\tilde{u}\}_{i+1} = \{u\}_i + \Delta t\{v\}_i + \frac{1}{2}\Delta t^2(1-2\beta)\{a\}_i \tag{19}$$

$$\{\tilde{v}\}_{i+1} = \{v\}_i + \Delta t(1-\gamma)\{a\}_i \tag{20}$$

Here, $\{\tilde{u}\}$ and $\{\tilde{v}\}$ are the estimated displacement and velocity vectors, respectively. Eqs. (21) and (22) are obtained by substituting Eqs. (19) and (20) into Eqs. (15) and (16).

$$\{u\}_{i+1} = \{\tilde{u}\}_{i+1} + \beta\Delta t^2\{a\}_{i+1} \tag{21}$$

$$\{v\}_{i+1} = \{\tilde{v}\}_{i+1} + \Delta t\gamma\{a\}_{i+1} \tag{22}$$

After these equations are substituted into Eq. (17), the numerical integration is performed. The procedure for the numerical integration algorithm and the flow diagram for the dynamic analysis of the structural system are presented in Figs. 7 and 8.

4. Numerical application

A program that can perform linear and non-linear dynamic analyses of masonry walls was written in this study. The program was written in MATLAB. In addition, a mesh program that can draw walls of the desired dimensions was written in MATLAB and can mesh the wall into the desired number of elements. The mesh program can model masonry walls separately as brick and mortar. Node coordinates, element and node numbers, element connectivity, restrained nodes and material properties are prepared with the mesh program as the input file for the main program. The main program begins the analysis using this prepared input file. Quadrilateral elements, with four nodal points and two degrees of freedom on each nodal point, were used in the analyses. Element stiffness matrixes were found using 2x2 Gauss integration rule. The strain of elements at each integration point was calculated, and the principal strain was obtained through this strain. All the element dimensions were chosen in a way that does not to exceed the maximum acceptable dimension criteria. The characteristic element dimension (l_{ch}) was calculated by taking the square root of the calculated area at each integration point. The finite element solution process of the system was initiated with an uncracked material elastic stiffness matrix. The iteration procedure was initiated choosing the integration point of the element that has the highest tensile strain energy ($\sigma_i\ \varepsilon_i\ /2$) among all element integration points, where softening may occur. The analysis was continued using the integration point of the element that has the highest strain among the uncracked elements at each iteration. The crack propagation on the wall was obtained using the integration point of a newly softening element at each iteration. The linear and non-linear dynamic analyses of a masonry wall with window opening were performed. In this study, micro modelling technique was used for the analysis of the masonry wall. It is accepted that the potential cracks would be occurred in the mortar and brick. The interface is assumed as a bond between mortar and brick. In the finite element mesh of the model, 720 nodal points and 648 quadrilateral elements were used. Brick with dimensions of 30x13.5x19 cm^3 and mortar with a thickness of 1.5 cm were used to model the wall. The modulus of elasticity, Poisson's ratio, mass per volume, tensile

strength and fracture energy for the brick to be used in the masonry wall were received set as $19x10^5$ N/cm^2, 0.20, $1.8x10^{-3}$ kg/cm^3, 220 N/cm^2 and 1.5 N/cm, respectively. For the mortar material, the values for the modulus of elasticity, Poisson's ratio, mass per volume, tensile strength and fracture energy were $16x10^5$ N/cm^2, 0.20, $1.6x10^{-3}$ kg/cm^3, 180 N/cm^2 and 1 N/cm, respectively. The degrees of freedoms, in the x and y directions, of all nodal points at the base of the model, in the y direction, and the nodal points at the top of the wall were constrained. The static solutions under the effect of system's own weight were considered as the initial conditions in the dynamic analyses. The number of studies about damping coefficient is limited (Bayraktar *et al.* 2014). A stiffness proportional damping matrix was used in the calculations. The damping coefficient was calculated by taking 5% of the damping ratio in the wall's fundamental mode. For the dynamic analysis, the acceleration records of the earthquake that occurred in Erzincan on 13 March, 1992, with the magnitude of 6.8, were used. The time step of the earthquake acceleration records is 0.01 s. Integration time step was chosen as 0.001 s. The numerical damping parameter α that is used in the HHT-α method was taken as -0.1. The peak acceleration values of the Erzincan earthquake in the east-west, north-south and vertical directions are 0.50g, 0.40g and 0.25g, respectively. In Fig. 9, the acceleration records of the earthquake are given, respectively for the east-west, north-south and vertical directions.

In addition, the acceleration records of the Bingöl earthquake, which occurred on 1 May, 2003, with a magnitude of 6.1, were also used to investigate different earthquake effects on the model. The peak acceleration values of the Bingöl earthquake in the east-west, north-south and vertical directions are 0.50g, 0.40g and 0.25g, respectively. The acceleration records of the Bingöl earthquake are presented in Fig. 10.

For the linear and non-linear dynamic analysis, the east-west and vertical acceleration components of the Erzincan earthquake were applied in the x and y direction of the model, respectively. The finite element mesh of the model is given in Fig. 11. One nodal point (645) and four integration points (A, B, C and D) are marked on the finite element mesh of the masonry wall to plot the time history of the displacement and principal stress.

Linear and non-linear solutions of the horizontal and vertical displacement values, obtained at nodal point 645, are presented in Fig. 12.

When linear and non-linear solutions are compared, it can be seen that the values of displacement had the same values until t=2.56 s, when the first crack occurred; subsequently, the graphs had separated from each other with increased cracking in the model. A comparison of the absolute maximums of the horizontal and vertical displacement values, obtained from linear and non-linear analyses, illustrates that the non-linear solutions are larger and that the differences between them are approximately 12% and 28%, respectively. The time history graphs of the maximum and minimum principal stress, obtained at integration points A, B, C and D, are given in Figs. 13-16, respectively. As the time history graphs of the stress shows similarity, increases or decreases occur at their amplitudes. Examination of the non-linear solutions illustrates that the peak values of the maximum principal stress were less than the tensile strength of the material.

The results of the non-linear dynamic analysis showed that, the first crack in the model occurred at the upper-left corner of the window opening on the wall at t=2.56 s. The number of cracked elements is increased in later time steps, and the cracks are expanded. Cracked elements may become enclosed and reopen at various times during the analysis. Cracks occur at the other corners of the window opening at subsequent time steps, and they expanded diagonally. Crack propagations at times of t=3.0 and 4.5 s are shown in Fig. 17. An apparent increase was not observed in the wall at subsequent time steps.

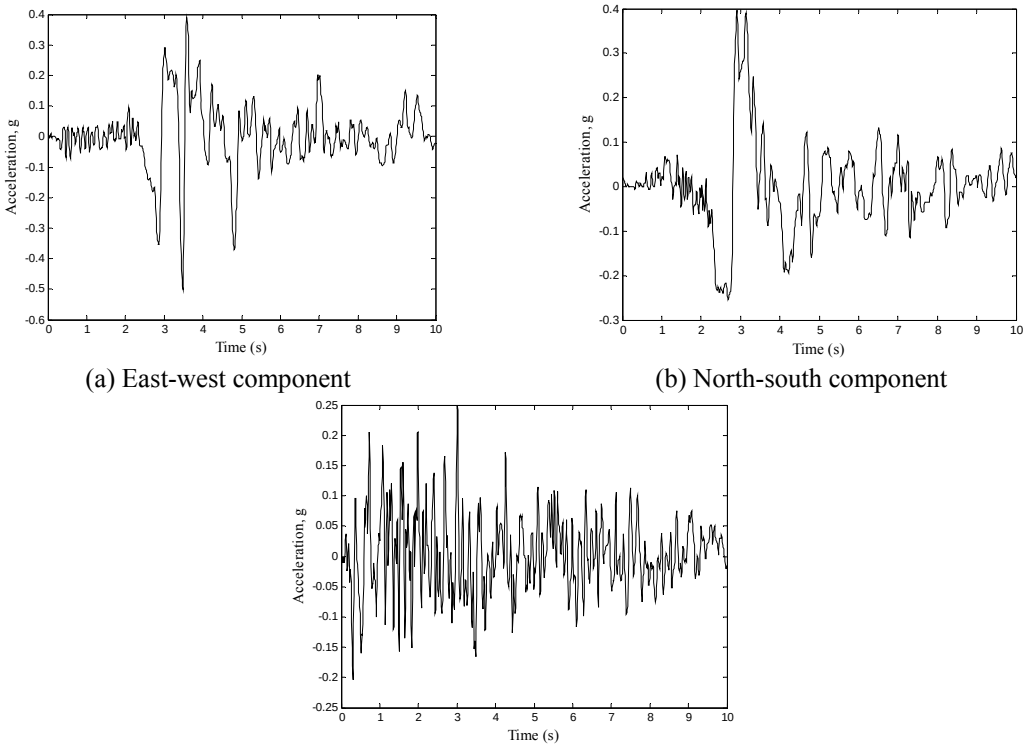

(a) East-west component (b) North-south component

(c) Vertical component

Fig. 9 Erzincan earthquake acceleration records

For the second linear and non-linear dynamic analysis, the east-west and vertical acceleration components of the Bingöl earthquake were applied in the x and y directions of the model, respectively. The acceleration records of the Bingöl earthquake are shown in Fig. 10. The time history graphics of nodal point 645 are presented in Fig. 18 based on the results of the linear and non-linear analyses. The displacement, in the linear and non-linear solutions, had the same values until t=1.70 s, when the first crack occurred; subsequently, the graphs separate from each other with increased cracking in the model. A comparison of the absolute maximums of the horizontal and vertical displacements obtained from linear and non-linear analyses indicates that the differences between them were 31% and 28%, respectively.

Time histories of the maximum and minimum principal stress, obtained at integration points A, B, C and D are given in Figs. 19-22, respectively. The peak values of the maximum principal stress were less than the tensile strength of the material when considering the non-linear solutions.

The results of the non-linear dynamic analysis showed that, the first crack in the model occurred at the upper-right corner of the window opening on the wall at t=1.70 s. The number of cracked elements increase in later time steps of the analysis, and the crack expands depend on the earthquake effect. Cracked elements may close and reopen at various times of the analysis. Cracks occur at the other corners of the window opening at later time steps, and they proceed diagonally. Crack propagations at times of t=3.0 and 4.5 s are shown in Fig. 23.

No significant increase in the crack propagation was observed in the subsequent time steps. The solutions obtained for the Bingöl and Erzincan earthquakes were compared to each other;

variations can be observed in the time history of the displacement (both in frequency and amplitude) and crack intensity obtained in damage areas. In addition, the first cracks that occurred on the walls exhibit variations with regards to their locations and times.

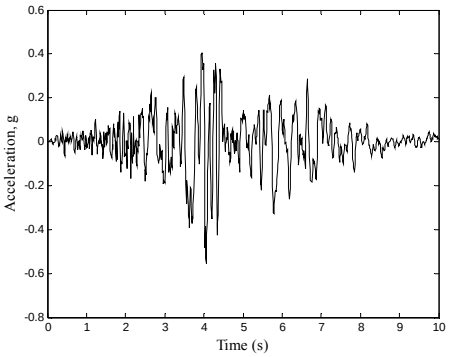

(a) East-west component

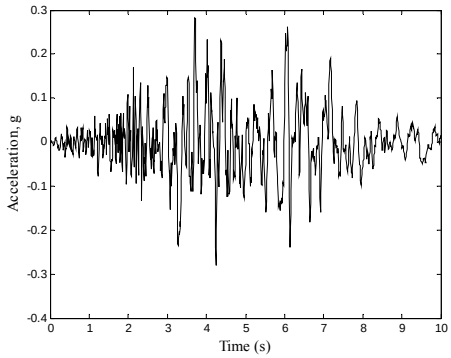

(b) North-south component

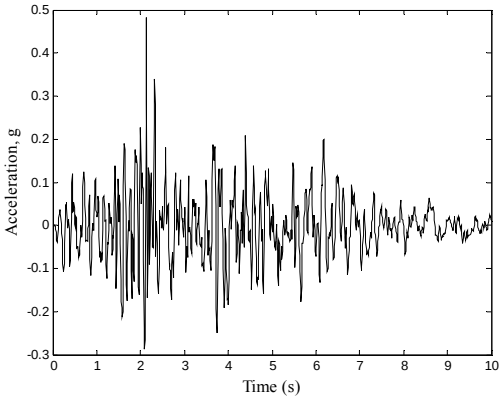

(c) Vertical component

Fig. 10 Bingöl earthquake acceleration records

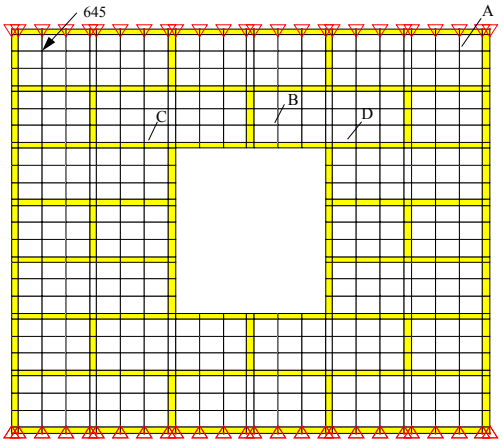

Fig. 11 Finite element mesh of the masonry wall

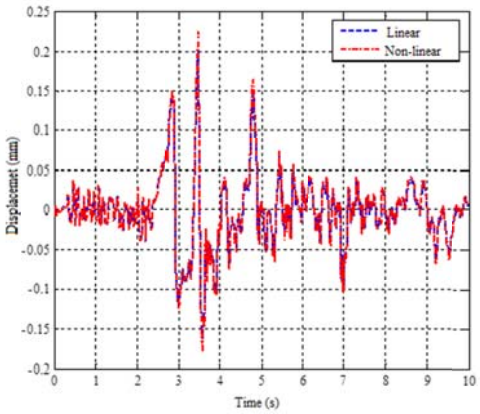

(a) Horizontal displacement

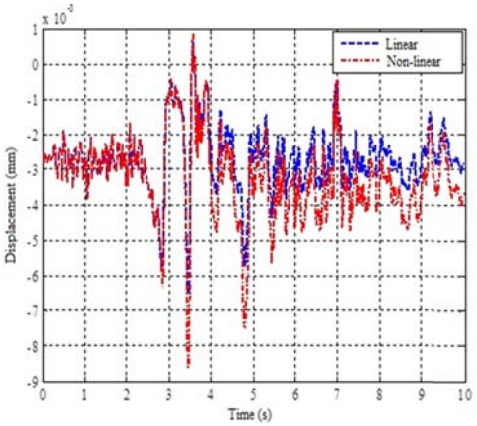

(b) Vertical displacement

Fig. 12 Time histories of the displacement at nodal point 645 (Erzincan earthquake)

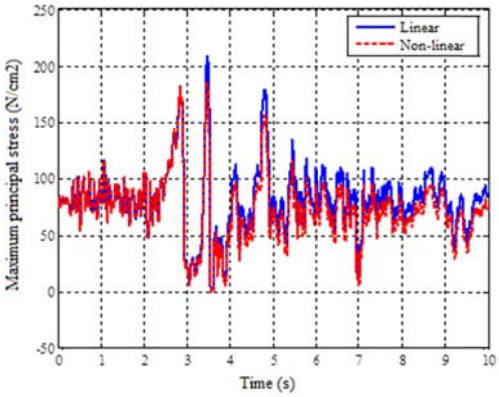

(a) Maximum principal stress

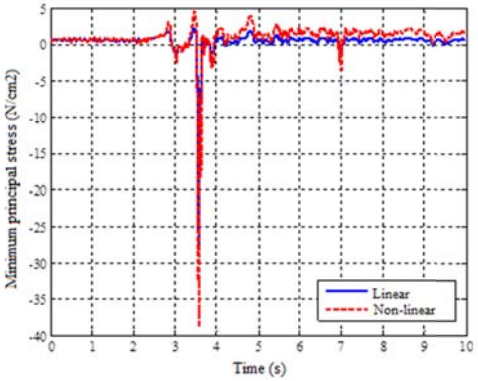

(b) Minimum principal stress

Fig. 13 Time histories of the principal stress that occurred at integration point A (Erzincan earthquake)

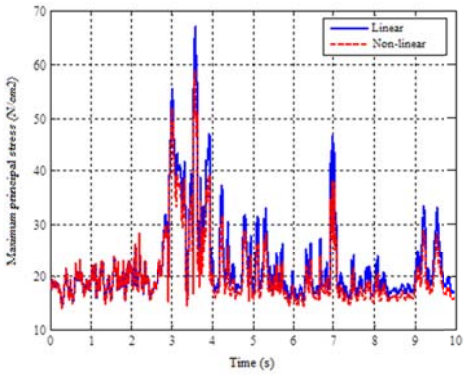

(a) Maximum principal stress

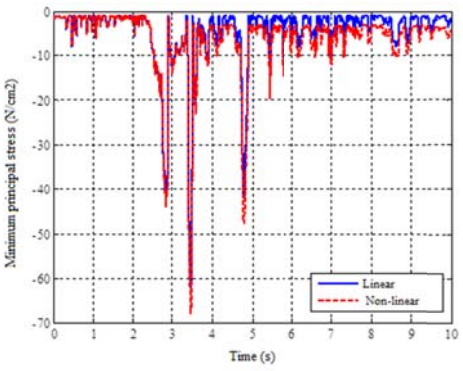

(b) Minimum principal stress

Fig. 14 Time histories of the principal stress that occurred at integration point B (Erzincan earthquake)

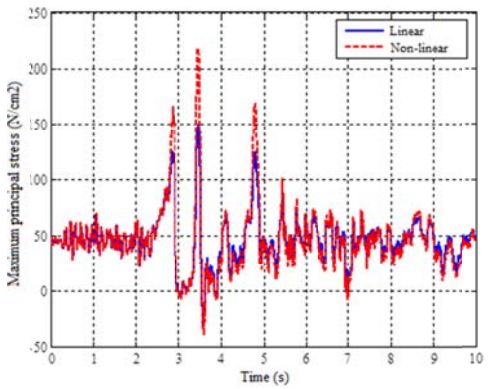

(a) Maximum principal stress

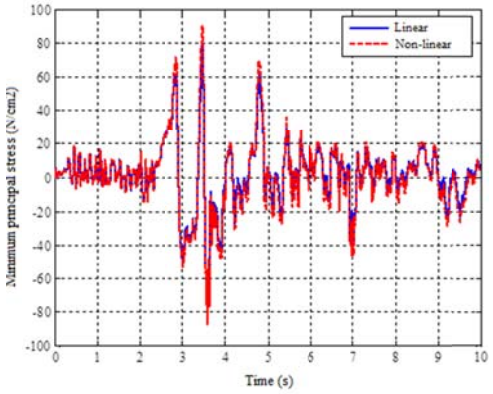

(b) Minimum principal stress

Fig. 15 Time histories of the principal stress that occurred at integration point C (Erzincan earthquake)

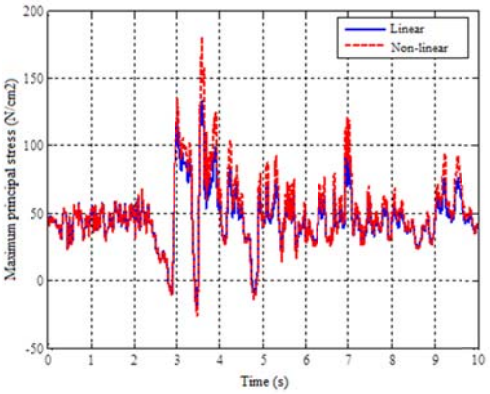

(a) Maximum principal stress

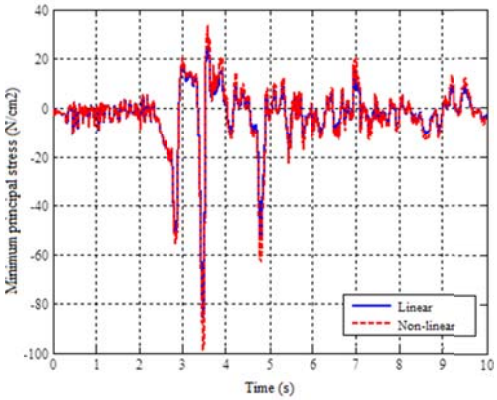

(b) Minimum principal stress

Fig. 16 Time histories of the principal stress that occurred at integration point D (Erzincan earthquake)

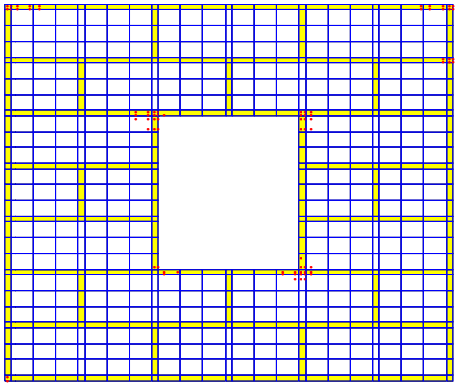

(a) t =3.0 s

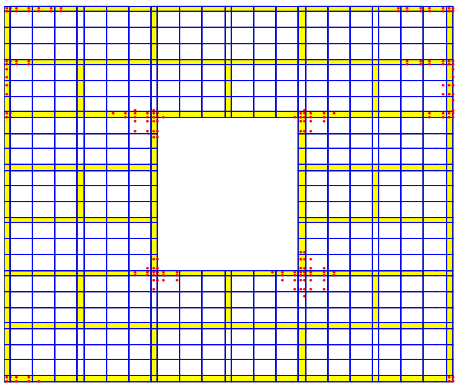

(b) t= 4.5 s

Fig. 17 Crack propagation (Erzincan earthquake)

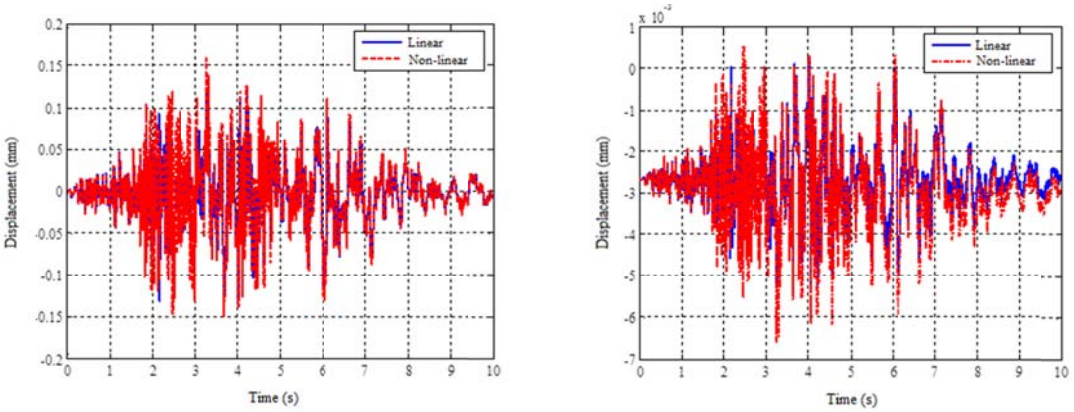

(a) Horizontal displacement (b) Vertical displacement

Fig. 18 Time histories of the displacement of nodal point 645 (Bingöl earthquake)

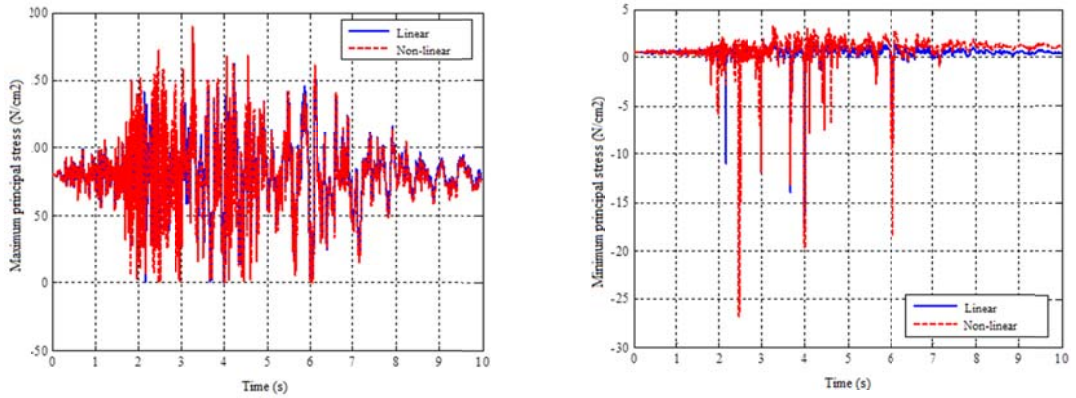

(a) Maximum principal stress (b) Minimum principal stress

Fig. 19 Time histories of the principal stress that occurred at integration point A (Bingöl earthquake)

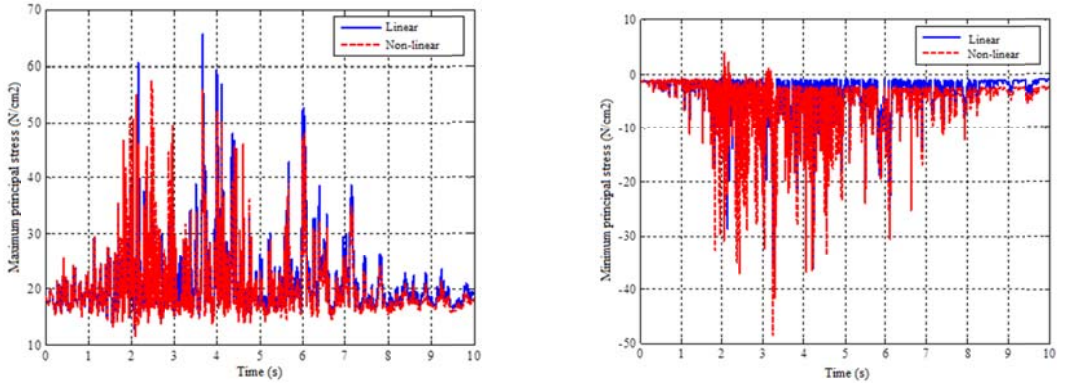

(a) Maximum principal stress (b) Minimum principal stress

Fig. 20 Time histories of the principal stress that occurred at integration point B (Bingöl earthquake)

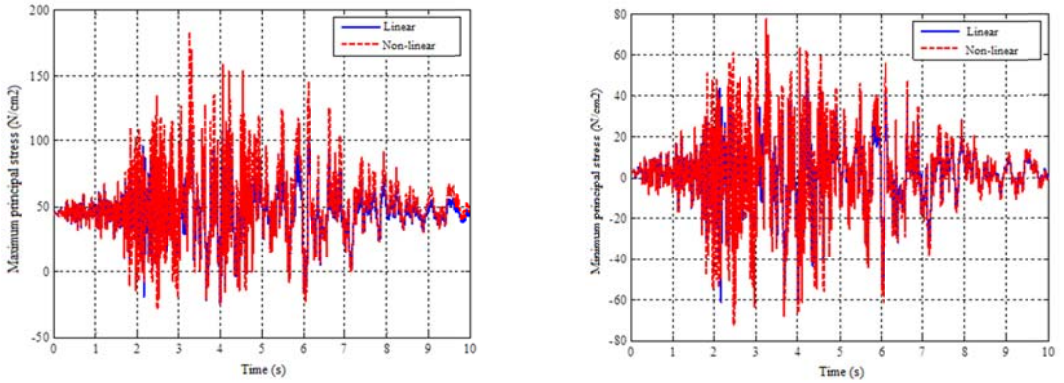

(a) Maximum principal stress (b) Minimum principal stress

Fig. 21 Time histories of the principal stress that occurred at integration point C (Bingöl earthquake)

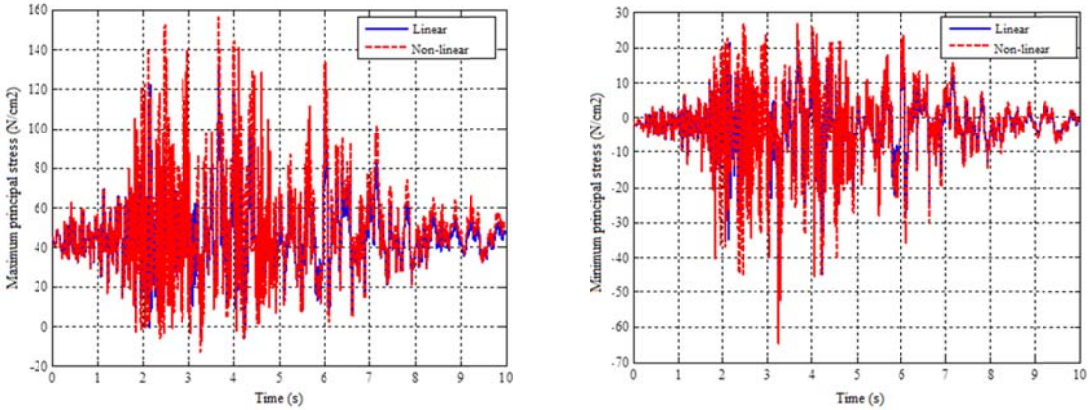

(a) Maximum principal stress (b) Minimum principal stress

Fig. 22 Time histories of the principal stress that occurred at integration point D (Bingöl earthquake)

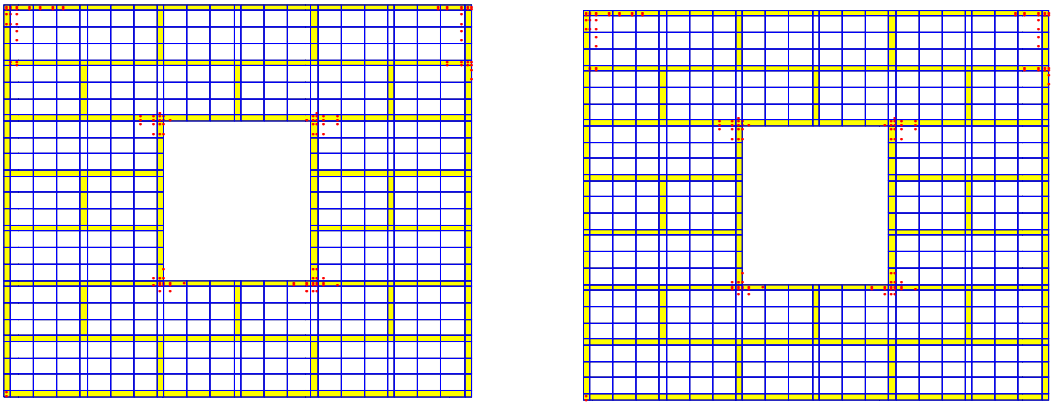

(a) t = 3.5 s (b) t = 4.5 s

Fig. 23 Crack propagation (Bingöl earthquake)

5. Conclusions

In this study, linear and non-linear dynamic analysis of a masonry wall that includes an opening was performed. For this purpose, a program that can perform linear and non-linear dynamic analyses of masonry walls was written. Furthermore, a mesh program was written that can mesh the wall into the desired number of elements. Smeared crack model that includes the strain softening behavior was selected for the masonry material. For the numerical application, linear and non-linear dynamic analyses of the two-dimensional masonry wall were carried out using acceleration records obtained from the 1992 Erzincan and 2003 Bingöl earthquake. Crack propagation in the wall was investigated. Cracks first occur at the corners of the window openings and expand between window openings and wall corners depend on the dynamic effect. When the obtained solutions were analyzed, it was seen that the peak values of maximum principal stresses in linear state exceeded the tensile strength of the material and could cause tensile fracture in the material and the peak values of minimum principal stresses remained under the compressive strength of the material. It was seen that linear and non-linear dynamic solutions were the same until the first crack was formed on the masonry wall when time histories of the displacement and principal stress were investigated for both earthquake acceleration records. The differences between the linear and non-linear solutions became apparent with an increasing number of cracks. Frequency, amplitude quantities and crack intensity occurred in damage areas show differences when the solutions obtained for 1992 Erzincan and 2003 Bingöl earthquakes were compared to each other. Finally, earthquake characteristics significantly affect the solutions.

References

Bayraktar, A., Coşkun, N. and Yalçın, A. (2007), "Damages of masonry buildings during the July 2, 2004 Dogubayazıt (Ağrı) earthquake in Turkey", *Eng. Fail. Anal.*, **14**(1), 147-157.

Bayraktar, A., Şahin, A., Özcan, D. and Yıldırım, F. (2010), "Numerical damage assessment of Hagia Sophia bell tower by nonlinear FE modelling", *Appl. Math. Model.*, **34**(1), 92-121.

Bayraktar, A., Türker, T. and Altunışık, A.C. (2015), "Experimental frequencies and damping ratios for historical masonry arch bridges", *Constr. Build. Mater.*, **75**(30), 234-241.

Bazant, Z.P. and Cabot, G.P. (1989), "Measurement of characteristic length of nonlocal continuum", *J. Eng. Mech.*, **115**(4), 754-766.

Bernardeschi, K., Padovani, C. and Pasquinelli, G. (2004), "Numerical modeling of the structural behavior of Buti's bell tower", *J. Cult. Herit.*, **5**(4), 371-378.

Building Census (2000), State Institute of Statistics Prime Ministry Republic of Turkey, Ankara, Turkey.

Calayır, Y., Sayın, E. and Yön, B. (2012), "Performance of structures in the rural area during the March 8, 2010 Elazığ -Kovancılar earthquake", *Nat. Hazards.*, **61**(2), 703-717.

Carpinteri, A., Invernizzi, S. and Lacidogna, G. (2005), "In situ damage assessment and nonlinear modelling of a historical masonry tower", *Eng. Struct.*, **27**(3), 387-395.

Erdik, M. and Aydınoğlu, N. (2003), "Earthquake vulnerability of buildings in Turkey", *Proceedings of the 3rd International Symposium on Integrated Disaster Risk Management,* Kyota, Japan, July.

Ingham, J. and Griffith, M. (2011), "Performance of unreinforced masonry buildings during the 2010 Darfield (Christchurch, NZ) earthquake", *Aust. J. Struct. Eng.*, **11**(3), 1-18.

Ivorra, S., Pallares, F.J., Adam, J.M. and Tomas, R. (2010), "An evaluation of the incidence of soil subsidence on the dynamic behaviour of a Gothic bell tower", *Eng. Struct.*, **32**(8), 2318-2325.

Klingner, R.E. (2006), "Behavior of masonry in then Northridge (US) and Tecoma´n–Colima (Mexico) earthquakes: Lessons learned, and changes in US design provisions", *Constr. Build. Mater.*, **20**(4),

209-219.
Lofti, H.R. and Shing, P.B. (1991), "An appraisal of smeared crack models for masonry shear wall analysis", *Comput. Struct.*, **41**(3), 413-425.
Lubliner, J., Oliver, J., Oller, S. and Onate, E. (1989), "A plastic damage model for Concrete", *Int. J. Solids. Struct.*, **25**(3), 299-326.
Lourenço, P.B. (1996), "Computational strategies for masonry structures", Ph.D. Thesis, Delft Technical University of Technology, The Netherlands.
Miranda, I., Ferencz, R.M. and Hughes, T.J.R. (1989), "An improved implicit–explicit time integration method for structural dynamics", *Earthq. Eng. Struct. D.*, **18**(5), 643–653.
Modena, C., Valluzzi, M.R., Folli, R. and Binda, L. (2002), "Design choices and intervention techniques for repairing and strengthening of the Monza cathedral bell-tower", *Constr. Build. Mater.*, **16**(7), 385-395.
Naseer, A., Khan, A.N., Hussain, Z. and Ali, Q. (2010), "Observed seismic behavior of buildings in Northern Pakistan during the 2005 Kashmir earthquake", *Earthq. Spectra.*, **26**(2), 425-449.
Oliver, J. (1989), "A Consistent Characteristic Length for Smeared Cracking Models", *Int. J. Numer. Meth. Eng.*, **28**, 461-474.
Rots, J, G. (1988), "Computational modelling of concrete fracture", Thesis Report, Civil Engineering Department of Delft University.
Rots, J, G. (1991), "Numerical simulation of cracking in structural masonry", *Heron*, **36**(2), 49-63.
Rots, J.G. (1997), "Structural Masonry", TNO Building and Construction Research, Netherlands, 152.
Sayın, E., Yön, B., Calayır, Y. and Karaton, M. (2013), "Failures of masonry and adobe buildings during the June 23, 2011 Maden-(Elazığ) earthquake in Turkey", *Eng. Fail. Anal.*, **34**, 779-791.
Sayın, E., Yön, B., Calayır, Y. and Gör, M. (2014), "Construction failures of masonry and adobe buildings during the 2011 Van earthquakes in Turkey", *Struct. Eng. Mech.*, **51**(3), 503-518.
Shing, P.B. and Cao, L. (1997), "Analysis of partially grouted masonry shear walls", Department of Civil. Environmental & Architectural Engineering, University of Colorado, 46.
Skrikerud, P.E. and Bachmann, H. (1986), "Discrete crack modeling for dynamically loaded unreinforced concrete structures", *Earthq. Eng. Struct. D.*, **14**(2), 297-315.
Unnikrishnan, S., Narasimhan, M.C. and Venkataramana, K. (2013), "Effect of containment reinforcement on the seismic response of box type laterite masonry structures – an analytical evaluation", *Earthq. Struct.*, **5**(1), 67-81.

CC